Mon. Not. R. Astron. Soc. **000**, 1–14 (2007) Printed 2 April 2008 (MN LATEX style file v2.2)

High Dispersion Absorption-line Spectroscopy of AE Aqr

J. Echevarría,[1⋆] Robert Connon Smith,[3] R. Costero,[1] S. Zharikov,[2] R. Michel[2]
[1] *Instituto de Astronomía, Universidad Nacional Autónoma de México, Apartado Postal 70-264, México, D.F., 04510, México*
[2] *Instituto de Astronomía, Universidad Nacional Autónoma de México, Apartado Postal 877, Ensenada, Baja California, 22800, México*
[3] *Department of Physics & Astronomy, University of Sussex, Falmer, Brighton, Sussex BN1 9QH, UK*

Accepted 2008 xxxxx. Received 2 April 2008

ABSTRACT

High-dispersion time-resolved spectroscopy of the unique magnetic cataclysmic variable AE Aqr is presented. A radial velocity analysis of the absorption lines yields $K_2 = 168.7 \pm 1\,\mathrm{km\,s^{-1}}$. Substantial deviations of the radial velocity curve from a sinusoid are interpreted in terms of intensity variations over the secondary star's surface. A complex rotational velocity curve as a function of orbital phase is detected which has a modulation frequency of twice the orbital frequency, leading to an estimate of the binary inclination angle that is close to 70°. The minimum and maximum rotational velocities are used to indirectly derive a mass ratio of $q = 0.6$ and a radial velocity semi-amplitude of the white dwarf of $K_1 = 101 \pm 3\,\mathrm{km\,s^{-1}}$. We present an atmospheric temperature indicator, based on the absorption line ratio of Fe I and Cr I lines, whose variation indicates that the secondary star varies from K0 to K4 as a function of orbital phase. The ephemeris of the system has been revised, using more than one thousand radial velocity measurements, published over nearly five decades. From the derived radial velocity semi-amplitudes and the estimated inclination angle, we calculate that the masses of the stars are $M_1 = 0.63 \pm 0.05\,\mathrm{M_\odot}$; $M_2 = 0.37 \pm 0.04\,\mathrm{M_\odot}$, and their separation is $a = 2.33 \pm 0.02\,\mathrm{R_\odot}$. Our analysis indicates the presence of a late-type star whose radius is larger, by a factor of nearly two, than the radius of a normal main sequence star of its mass. Finally we discuss the possibility that the measured variations in the rotational velocity, temperature, and spectral type of the secondary star as functions of orbital phase may, like the radial velocity variations, be attributable to regions of enhanced absorption on the star's surface.

Key words: binaries: close – stars: individual: AE Aqr – stars: novae, cataclysmic variables – stars: rotation

1 INTRODUCTION

Cataclysmic variables are semi-detached binary systems in which a red dwarf secondary loses material through the inner Lagrangian point into an accretion disc, ring or accretion column around the white dwarf primary. The secondary stars in cataclysmic variables are challenging targets to study because their spectrum is heavily veiled by the strong blue continuum of the accretion disc. Since the donor star is an important piece in the understanding of these interacting binaries, it is paramount to make detailed and high quality spectroscopic studies of their secondary stars.

AE Aquarii is an 11-12 mag cataclysmic variable, which was discovered in the optical by Zinner (1938). It is located at about 100 pc (Friedjung 1997) and was first associated with the DQ Her or *Intermediate Polar* stars by Patterson (1979). Its binary nature was discovered by Joy (1954), who found this system to be consistent with a small hot star and a late-type companion of spectral type dK0, with an orbital period of about 16.84 hr. A corrected period, of around 9.88 hr, was obtained later by Walker (1965). Since AE Aqr is not an eclipsing system, its inclination angle is not well determined, but it is thought to be $i \approx 60° \pm 10°$, while its mass ratio is in the range $0.6 \leqslant q \leqslant 0.84$ (Patterson 1979; Chincarini & Walker 1981; Robinson, Shafter & Balachandran 1991; Reinsch & Beuermann 1994; Welsh, Horne & Gomer 1995; Casares et al. 1996; Watson, Dhillon & Shahbaz 2006; this paper). The absorption lines from the secondary star are very strong. The light curve of AE Aqr exhibits large flares and coherent oscillations of about 16 and 33 s in the optical and X-ray (Patterson 1979). It also exhibits radio and millimetre synchrotron emission (e.g. Book-

⋆ jer@astroscu.unam.mx

binder & Lamb 1987; Bastian, Dulk & Chanmugam 1988), as well as TeV γ-rays (Bowden et al. 1992; Meintjes et al. 1992). The Balmer emission lines vary both in strength and shape and they may not be good tracers of the orbital motion of the white dwarf. This has led to the proposal of the magnetic propeller model (Wynn, King & Horne 1997).

The study of the physical conditions in the intermediate polar AE Aqr is important because the system shows some remarkable and unique features. Understanding the behaviour of this binary may help us to understand, for example, the role that mass transfer has in this kind of binary (Watson et al. 2006). Obtaining accurate masses in this system is also an important goal. Because the secondary spectrum is clearly visible, it is possible to determine a reliable value for K_2, as we do below. In AE Aqr, an unstable accretion disc is present, which makes direct observations of the radial velocity semi-amplitude of the accretion disc difficult and, consequently, the direct determination of the real K_1 value is unreliable. One indirect method of determining K_1 is to use the orbital variations in the spin pulse of the rapidly rotating white dwarf (Robinson et al. 1991). However, given that the secondary star shows a clearly measurable rotational velocity, an alternative way of determining the mass ratio is by combining the K_2 value with the rotational velocity of the late-type star (Horne, Wade & Szkody 1986). It is then possible to deduce the value of K_1, and use it, along with our measured value of K_2 and our estimate of the inclination, to calculate the individual stellar masses (cf. Section 9).

Detailed radial velocity studies of the secondary star were first made by Chincarini & Walker (1981) and later by Robinson et al. (1991), Reinsch & Beuermann (1994), Welsh et al. (1995), Casares et al. (1996) and Watson et al. (2006). We present here observations of AE Aqr, made with the UCL echelle spectrograph (UCLES) at the Anglo Australian Telescope and with the Echelle spectrograph at the San Pedro Mártir Observatory in México. In this first paper, we concentrate on the radial velocity analysis of the absorption lines and compare our results with previous studies. In a later paper, after obtaining further observations, we will deal with the complex emission lines, whose analysis imposes significant challenges; the lines sometimes appear to come from fragmented material orbiting the white dwarf, while at other times they show the presence of a full accretion disc.

2 OBSERVATIONS

Spectroscopic observations of AE Aqr were made using the Anglo-Australian Telescope (AAT) and the University College London Echelle Spectrograph (UCLES) at the coudé focus on 1991 August 2 and 3. We obtained 102 spectra, 360 s exposure each, with a typical signal-to-noise ratio of 10 (around λ4500 Å). We used the 31.6 lines mm^{-1} grating and the Blue Thomson 1024×1024 CCD with the 700 mm camera. The spectral region λ4000 Å to λ5100 Å was covered. The spectral resolution was about 5.4 km s^{-1}. Almost two complete orbital periods were covered. Several late-type template stars were also observed.

Three further runs were obtained at the Observatorio Astronómico Nacional at San Pedro Mártir (SPM) using the 2.1m Telescope and the Echelle Spectrograph. The first observations were gathered on the nights of 1997 September 22 and 23. We obtained 18 spectra, 600 s exposure, with typical signal-to-noise ratio of 25 (around λ5450 Å). We used the 15μm Thomson 2048×2048 detector, with the 300 lines mm^{-1} echellette grating to cover a spectral range from λ3400 Å to λ7300 Å. The spectral resolution for this configuration was about 15.4 km s^{-1}. Orbital phases 0.37 – 0.55 (first day) and 0.58 – 1.00 (second day) were covered in this run. In the second set of observations, made on the nights of 2000 August 17 to 19, 81 spectra of 600 s exposure were obtained. The instrumental setup was similar to the first one, except that we covered a spectral range from λ3700 Å to λ7700 Å. Orbital phases $0.35-0.90$, $0.58-1.36$ and $0.0-0.73$ were covered on successive days with a typical signal-to-noise ratio of 42 (around λ 5450 Å). The third run was made on 2001 August 29, when 47 spectra were obtained with shorter exposure times of 180 s with a typical signal-to-noise ratio of 28 (around λ5450 Å). We used the 24μm SITe 1024×1024 detector, with a configuration to cover a spectral range from λ3900 Å to λ7100 Å. The spectral resolution for this configuration is about 24.6 km s^{-1}. Only two spectral type standards, 61 Cygni A and B, were observed during the SPM runs.

The list of observed standards is shown in Table 1. Most of these stars are not primary standards. Their spectral classifications (column 3) have been taken mainly from the Bright Star Catalogue and updated from several sources (see references in the Table). Their radial velocities are also shown; these values have been obtained from a variety of sources, as listed in the Table references. We have also derived our own radial velocity measurements (column 5), and have cross-correlated the results to check for inconsistencies. In general there is a good agreement among all sources and we have adopted the values given in column 4. The published rotational velocities, not listed, all have very low values, less than our spectral resolution of 10 km s^{-1}, as expected in general from isolated cool main-sequence stars.

3 DATA REDUCTION AND SPECTRAL FEATURES

The AAT and SPM spectra were treated in a similar manner. They both have high dispersion orders separated by a cross-disperser, which have to be first extracted into one dimensional spectra, wavelength calibrated separately and then merged into a single array and re-binned to a single linear dispersion. The great stability of both UCLES and the Echelle Spectrograph allows us to interpolate with ease the calibration lamp spectra taken during the observing nights. The AAT spectra were reduced with STARLINK software and the SPM observations were reduced with the NOAO/IRAF V2.11 package[1].

The spectra of AE Aqr (e.g. Casares et al. 1996) show complex Hβ and Hγ emission lines and a weak HeI λ4471, superimposed on a red continuum with strong absorption lines, mainly from FeI, CrI, CaI, and MnI. As discussed in

[1] IRAF is distributed by the National Optical Astronomical Observatories, operated by the Association of Universities for Research in Astronomy, Inc., under cooperative agreement with the National Science Foundation.

Table 1. Parameters of Spectral Type Template Stars

Name	Henry Draper	Spectral Type	V_{Rad} ($km\,s^{-1}$)	$(V_{Rad})^4$	Ref[a]
–21 4065	HD135534	K2 III	–5.3	–9.7	a,1
36 Lib	HD138688	K3 III	12.3	6.1	b,1
36 Oph A	HD155886	K0 V	–0.6	0.4	h,2
36 Oph B	HD155885	K2 V	0.0	–0.4	c,2 (col 3: G8 V)
3 Ser	HD135482	K0 III	–34.24	-	j,1
δ Oph	HD146051	M0.5 III	–19.9	–21.6	d,1
η Scl	HD2429	M2/M4 III	11.2	12.2	b,1
HR 1004	HD20729	M1 III	+15	11.7	a,1
HR 13	HD344	K1 III	+7	7.2	j,3
HR 222	HD4628	K2 V	–12.6	–9.8	e,1
HR 471	HD10142	K0 III	29.7	29.1	b,2
HR 487	HD10361	K0 V	19.5	20.8	h,2
HR 486	HD10360	K0 V	22.5	22.2	h,2
HR 54	HD1089	K3 III	–52	–51.6	j,3
HR 67	HD1367	K0 II	–9.4	–8.8	j,1
HR 753	HD16160	K3 V	23.4	24.4	g,1
κ Oph	HD153210	K2 IIIvar	–55.6	–57.2	i,1
61 Cyg A	HD201091	K5 V	–64.3	-	f,1
61 Cyg B	HD201092	K7 V	–63.5	-	f,1

[a] References to Spectral Types: (a) Houk & Smith-Moore 1988; (b) Houk 1982; (c) Wilson 1962; (d) Morgan & Keenan 1973; (e) Morgan, Keenan & Kellman 1943; (f) Johnson & Morgan 1953; (g) Roman 1955; (h) Evans, Menzies & Stoy 1957; (i) Roman 1952; (j) Hoffleit 1964. References to Radial Velocities: (1) Wilson 1953; (2) Evans 1967; (3) Flynn & Freeman 1993; (4) This paper. Note: The spectral type in the last column, given in parentheses, refers to the value derived in this paper.

the Introduction, we shall leave the emission lines to a later paper and concentrate here on the behaviour and interpretation of the absorption lines coming from the secondary star.

The radial velocities were obtained for all observations using the *fxc* routine from the *rv* package in IRAF. For the case of the AAT data we selected for analysis the spectral region λ4200 Å to λ4330 Å, while for the SPM data we selected the region λ4870 Å to λ5530 Å. The selected spectral regions in the AAT and SPM data are not the same. For the SPM data we have combined the echelle orders which, due to the instrumental setup, have the maximum fluxes, while in the case of the AAT data, we have selected a region where the free spectral ranges overlap; this also avoids contamination from the Hγ line. As we will show in the analysis, the different selection for the *blue* and *green* spectral regions contributes a check on the validity of the results. We made a check for consistency for the AAT and SPM data with all the template stars. The semi-amplitude of the secondary obtained from the different standards shows a range of about $3\,km\,s^{-1}$, with no obvious correlation with spectral type. The cross-correlation peaks obtained with the *fxc* routine were well fitted by Gaussian functions in all cases.

4 RADIAL VELOCITIES AND SPECTROSCOPIC ORBITAL PARAMETERS

The measured radial velocities are shown in Tables 2 and 3 for the AAT observations with respect to HR 222, one of the observed standards which has a K2 V spectral type, consistent with the observed spectral type (see section 8). The radial velocities for the SPM data are shown in Tables 4 to 7 with respect to 61 Cyg A.

To calculate the spectroscopic orbital parameters (assuming a circular orbit), we have used a least-squares program which simultaneously fits the four fundamental variables in the equation:

$$V(t)_{\rm abs} = \gamma + K_{\rm abs}\ \sin[(2\pi(t - HJD_{\odot})/P_{\rm orb})],$$

where $V(t)_{\rm abs}$ are the observed radial velocities; γ is the systemic velocity; $K_{\rm abs}$ is the semi-amplitude of the radial velocity curve; $HJD_{\odot}$ is the heliocentric Julian date of the inferior conjunction of the companion; and $P_{\rm orb}$ is the orbital period of the binary.

In Table 8 we show the orbital parameters calculated from the SPM and AAT data using 61 Cyg A and HR 222 standards, respectively. The results for the semi-amplitude are very similar for both. However, there is a significant difference in the systemic velocity, probably due to the uncertainties in the absolute radial velocities of the template stars. We will adopt the systemic velocity obtained through 61 Cyg A, since this is a well known primary standard star (e.g. Keenan & McNeil 1976; Morgan, Keenan & Kellman 1943), which has also been used as a template in previous studies of AE Aqr.

5 SEMI-AMPLITUDE OF THE SECONDARY

Figure 1 shows the radial velocity curves of the secondary, separately for the AAT (top) and SPM (bottom) data. The

Table 2. Radial velocities for AE Aqr for August 2, 1991

HJD (240000+)	Absorption ($km\,s^{-1}$)	σ
48470.9548	91.0710	6.851
48470.9601	96.3983	6.736
48470.9654	94.5199	6.826
48470.9707	96.6956	6.836
48470.9760	95.4723	7.065
48470.9813	95.0824	6.284
48470.9866	96.2528	6.969
48470.9919	91.3255	7.177
48470.9972	87.0076	7.091
48471.0025	81.8741	6.925
48471.0108	72.1152	7.950
48471.0161	65.8743	8.984
48471.0214	59.1111	10.617
48471.0267	53.4765	13.676
48471.0320	41.8962	10.892
48471.0373	31.6189	8.460
48471.0426	21.4795	7.380
48471.0479	10.5793	5.600
48471.0532	-0.8366	4.731
48471.0585	-15.2109	4.909
48471.0638	-28.1980	5.468
48471.0691	-39.2205	5.440
48471.0744	-54.6164	6.714
48471.0797	-71.7725	6.748
48471.0850	-89.5616	7.276
48471.0903	-107.0077	7.192
48471.0956	-119.2595	6.615
48471.1009	-134.7471	6.247
48471.1062	-147.4073	6.071
48471.1115	-157.5921	5.689
48471.1168	-169.2017	5.870
48471.1221	-179.3889	5.770
48471.1275	-188.2508	5.805
48471.1328	-193.2074	5.509
48471.1381	-202.0784	6.967
48471.1434	-208.8203	6.023
48471.1487	-213.4168	6.744
48471.1540	-218.1144	7.078
48471.1644	-228.3875	11.888

orbital phase was derived from the revised ephemeris in section 6. The symbols, corresponding to data from different nights, are explained in the figure caption. The error bars for the individual measurements are given in the third column of the Radial Velocity Tables. These are the errors on the centroid obtained by fitting a Gaussian to the cross-correlation peak in each spectrum. In general they are of the order of $7\,km\,s^{-1}$, although there are some points with errors significantly greater than this mean value. The sinusoidal (solid) curves have the corresponding semi-amplitude and systemic values given in Table 8.

At some orbital phases, the radial velocity points deviate from a sinusoid. In order to study these deviations more carefully, we have subtracted the sinusoidal fits described in the last paragraph and obtained a plot of the residual velocities, shown in Figure 2. For the AAT data (top panel), we observe a fairly clear double-peaked curve; for the SPM data (lower panel) the curve is noisier, but there is still a peak apparent at about phase 0.4, similar to the one in the

Table 3. Radial velocities for AE Aqr for August 3, 1991

HJD (240000+)	Absorption ($km\,s^{-1}$)	σ
48471.9201	-126.4122	8.231
48471.9259	-139.3585	8.008
48471.9312	-155.5876	7.838
48471.9366	-163.1004	7.653
48471.9419	-176.1589	6.416
48471.9472	-185.5920	6.677
48471.9525	-194.5284	6.225
48471.9578	-202.5913	6.497
48471.9631	-207.7151	7.276
48471.9684	-213.9204	6.869
48471.9737	-219.8087	6.796
48471.9791	-221.0292	7.845
48471.9844	-227.2314	7.481
48471.9897	-229.8207	7.022
48471.9950	-230.1261	6.794
48472.0003	-232.6394	7.163
48472.0079	-227.5887	6.922
48472.0132	-227.9404	7.330
48472.0185	-222.5029	7.479
48472.0239	-217.0616	7.229
48472.0292	-213.9255	6.978
48472.0345	-207.2891	6.660
48472.0398	-198.5409	6.446
48472.0451	-191.5137	6.657
48472.0504	-182.1613	6.712
48472.0557	-172.4799	7.469
48472.0610	-163.6605	7.279
48472.0663	-153.9607	7.165
48472.0718	-141.3581	7.079
48472.0771	-129.7343	6.812
48472.0824	-114.6732	6.248
48472.0896	-97.0794	6.813
48472.0949	-86.5703	6.533
48472.1002	-72.1837	5.909
48472.1055	-60.1698	6.059
48472.1108	-43.6431	6.745
48472.1161	-31.6927	5.927
48472.1214	-20.3661	7.159
48472.1267	-7.2741	6.957
48472.1321	0.7625	6.443
48472.1374	14.9686	6.286
48472.1427	24.2414	6.301
48472.1480	37.4443	5.874
48472.1533	42.5435	6.033
48472.1586	55.0288	5.722
48472.1639	64.6959	5.230
48472.1712	74.5404	5.386
48472.1765	80.6155	5.978
48472.1818	86.0617	5.159
48472.1872	90.5772	5.348
48472.1925	99.3953	6.555
48472.1978	98.4657	6.713
48472.2031	98.0316	6.387
48472.2084	99.6052	6.685
48472.2137	100.5013	6.638
48472.2191	99.5221	10.041
48472.2244	98.9665	8.874
48472.2297	95.5619	10.709
48472.2350	86.0348	14.289
48472.2403	83.6323	12.475
48472.2456	73.7468	8.801
48472.2509	67.5799	8.262
48472.2563	64.1177	8.744

Table 4. Radial velocities for AE Aqr for September 22-23, 1997

HJD (240000+)	Absorption ($km\,s^{-1}$)	σ
50713.7239	53.8834	6.056
50713.7434	17.1704	7.931
50713.7711	-57.9052	18.501
50713.7850	-91.7092	8.007
50713.7989	-124.5789	7.522
50714.6328	-160.4805	8.160
50714.6446	-180.6777	7.553
50714.6553	-201.3855	10.647
50714.6662	-213.5401	8.437
50714.6853	-231.5731	8.199
50714.6938	-234.5440	8.574
50714.7033	-238.4612	6.789
50714.7122	-231.7661	7.227
50714.7216	-228.0453	5.229
50714.7302	-221.1735	8.284
50714.7389	-209.9548	7.381
50714.7476	-188.2585	5.439
50714.8085	-49.6652	11.475

Table 5. Radial velocities for AE Aqr for August 17-18, 2000

HJD (240000+)	Absorption ($km\,s^{-1}$)	σ
51773.7263	65.2917	5.101
51773.7363	51.2997	3.848
51773.7459	36.9166	4.071
51773.7559	15.4658	2.995
51773.7655	-5.8116	3.193
51773.7751	-27.7636	3.297
51773.7901	-70.0045	6.230
51773.7997	-97.6795	6.767
51773.8093	-125.9648	4.670
51773.8191	-148.8826	4.394
51773.8287	-169.2657	4.268
51773.8383	-185.6042	4.281
51773.8699	-223.2806	3.845
51773.8794	-227.7806	4.271
51773.8891	-227.2547	4.247
51773.9045	-224.7867	5.136
51773.9141	-217.3888	4.857
51773.9237	-211.7197	6.597
51773.9340	-191.5169	4.304
51773.9436	-176.4511	4.720
51773.9532	-158.7131	5.179
51774.6477	-159.4111	4.662
51774.6669	-191.9790	4.974
51774.6769	-205.5982	5.558
51774.6865	-217.7922	4.667
51774.6961	-223.7707	4.932
51774.7100	-229.8889	5.784
51774.7196	-226.9689	5.189
51774.7292	-223.6042	4.290
51774.7390	-217.1240	4.296
51774.7486	-207.0125	4.437
51774.7582	-193.3962	4.688
51774.7689	-173.2024	3.150
51774.7786	-159.1386	4.645
51774.7881	-133.0462	3.750
51774.8047	-92.2058	4.272
51774.8143	-65.5297	3.668
51774.8239	-42.4604	3.638
51774.8341	-16.3695	4.008
51774.8437	5.6063	3.759
51774.8533	25.5118	4.780
51774.8636	48.4668	4.031
51774.8732	65.0504	4.190
51774.8828	76.6211	5.118
51774.8925	87.8831	6.009
51774.9021	95.6748	13.954
51774.9117	98.1195	14.311
51774.9261	94.3257	14.438
51774.9357	92.1290	7.321
51774.9453	83.7146	18.339
51774.9559	73.6381	5.081
51774.9655	63.6809	7.791

AAT data. For both sets of data, the peak is followed by a trough at around phase 0.6. This behaviour is very reminiscent of the residual velocity curves plotted by Davey & Smith (1992); in that paper, for the comparable disk systems with the best data, IP Peg and YY Dra, there is also a positive peak in the residuals plot at around phase 0.4 and a negative peak around phase 0.6. In the Davey & Smith (1992) paper, this behaviour was shown to correspond to asymmetric heating of the hemisphere of the star that faces the disk. That strongly suggests that this feature of the AE Aqr residual plots also arises from the fact that the hemisphere facing the disk is being heated. The fact that it occurs in both data sets suggests that it is a permanent feature of the system, as one might expect: the radiation source is there all the time, even if it may vary in strength.

The effect of heating is to reduce the absorption line strength on the heated inner hemisphere and so to increase the amplitude of the measured radial velocity curve, because the centre of light moves towards the averted hemisphere, away from the centre of mass. It is clear that a cool region of *enhanced* absorption line strength on the unheated outer hemisphere would also increase the amplitude, for the same reason, but that the effect on the residuals would now be centred roughly around the position of that region instead of around L_1. To a first approximation then, a region of greater absorption line strength would produce a second peak and trough about 0.5 in phase later than the one coming from the heated region and indeed we see in the AAT data a clear second rise and fall centred roughly on phase 1. This suggests that at the time of the AAT observations there was a fairly strong region of enhanced absorption somewhere on the unheated hemisphere, close to the 'anti-L_1 point' in longitude, although we can say nothing about latitude. The fact that we do NOT see a similar second peak in the SPM data would suggest that at the time of the SPM observations there was no such region (although, since the observations covered a much larger range of dates, we can't be so confident about that). A cool, dark feature that is only present on some occasions is reminiscent of the behaviour of sunspots, and our results may therefore be consistent with the tomographic observations of a 'star-spot' by Watson et al. (2006). However, our feature would produce an absorption dip in the

Table 6. Radial velocities for AE Aqr for August 19, 2000

HJD (240000+)	Absorption ($km\,s^{-1}$)	σ
51775.6393	-52.7959	3.865
51775.6489	-28.7739	3.291
51775.6585	-7.5620	4.793
51775.6681	13.4982	5.374
51775.6999	77.3029	6.634
51775.7095	86.5576	7.545
51775.7190	99.5335	10.032
51775.7353	106.2833	17.445
51775.7449	100.8198	17.871
51775.7545	98.0898	17.983
51775.7650	87.9296	20.548
51775.7746	82.2610	15.630
51775.7842	66.9225	12.160
51775.7979	47.5450	13.763
51775.8075	25.6446	12.399
51775.8171	11.6025	11.819
51775.8268	-13.1728	14.711
51775.8364	-40.5701	24.572
51775.8460	-62.9008	18.127
51775.8581	-97.6792	23.011
51775.8677	-123.7154	23.438
51775.8773	-144.6751	18.331
51775.8914	-176.1165	17.524
51775.9010	-192.9387	28.153
51775.9106	-209.5299	13.797
51775.9210	-214.6285	21.748
51775.9306	-227.1362	25.586
51775.9402	-229.8586	21.955

absorption lines rather than the emission bump seen in the tomography data, so the connection is not obvious.

6 EPHEMERIS REVISITED

Following the procedure of Welsh et al. (1995) we have extended the radial velocity data base, starting from the first measurements by Joy (1954) (105 points over the period 1943 to 1953), and including the measurements of Chincarini & Walker (1981) (250 points); Reinsch & Beuermann (1994) (40 points); Welsh et al. (1995) (197 points); Casares et al. (1996) (207 points); and this paper (247 points, the most recent in 2001). All data were carefully examined, checking for inconsistencies and typographical errors. In all we have included 1046 points covering 58 yr of observations. A data archive of the radial velocity data used here is available on request to us. We have included in our calculations the published errors of every measurement. In those cases where they have not been tabulated, we have taken mean values based on their spectral resolution and exposure times ($40\,km\,s^{-1}$ for Joy 1954 and $20\,km\,s^{-1}$ for Chincarini & Walker 1981). An improved orbital period of 0.4116554800 d was found. A new zero phase has been obtained using the SPM data with the new orbital period value. From these results we adopt the ephemeris

$$\mathrm{HJD} = 2,439,030.78496(9) + 0.4116554800(2)\mathrm{E}. \quad (1)$$

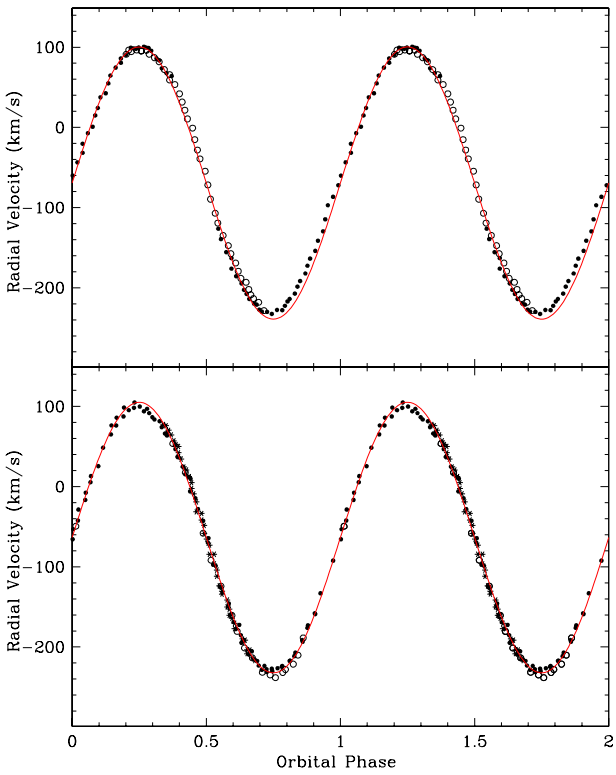

Figure 1. Radial velocity curves of the absorption lines of the secondary star. The upper plot shows the AAT data, where dots indicate night 1 and open circles night 2. The lower plot shows the SPM data, where dots indicate September 1997, open circles indicate August 2000 and asterisks August 2001. The solid curves are the sinusoidal fits defined by the parameters in Table 8.

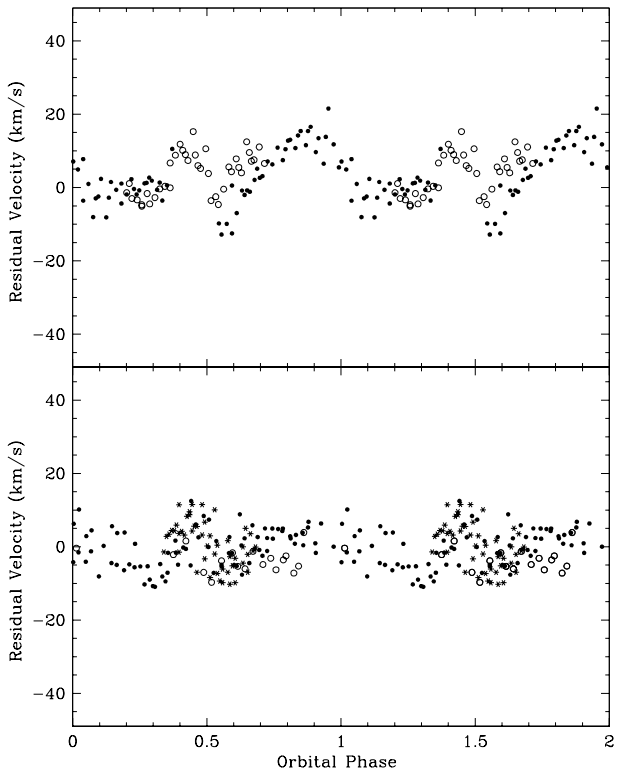

Figure 2. Residual velocities of the absorption lines of the secondary star. The plotted points are as described in Figure 1, but here we have subtracted the fitted sinusoid curves to show the deviations more clearly.

Table 7. Radial velocities for AE Aqr for August 29, 2001

HJD (240000+)	Absorption ($\mathrm{km\,s^{-1}}$)	σ
52150.8019	75.3120	4.437
52150.8047	69.5589	5.484
52150.8076	63.8477	4.453
52150.8104	56.6756	4.463
52150.8132	52.0995	4.274
52150.8160	49.3786	4.825
52150.8188	42.0882	5.078
52150.8217	36.1923	5.523
52150.8245	33.8993	6.534
52150.8273	24.1148	4.582
52150.8301	20.0940	5.016
52150.8330	11.8558	4.700
52150.8358	11.2627	3.945
52150.8386	4.2054	4.896
52150.8414	-2.7119	4.226
52150.8442	-9.1846	4.445
52150.8471	-19.7468	4.924
52150.8499	-32.0708	5.726
52150.8527	-34.3096	5.178
52150.8556	-42.5093	5.626
52150.8585	-49.2404	4.340
52150.8613	-59.2369	5.035
52150.8641	-66.0804	5.202
52150.8669	-73.8477	5.967
52150.8697	-84.9643	4.653
52150.8725	-85.0400	5.993
52150.8754	-96.7729	4.441
52150.8782	-104.3313	5.963
52150.8810	-112.2779	4.985
52150.8839	-123.8766	5.261
52150.8867	-130.6497	4.880
52150.8895	-134.5644	4.070
52150.8923	-141.7841	4.490
52150.8952	-150.4175	5.517
52150.8980	-153.4627	5.134
52150.9008	-160.6009	4.838
52150.9036	-164.4972	4.363
52150.9064	-171.1431	6.183
52150.9093	-177.4043	4.280
52150.9176	-190.1421	7.178
52150.9204	-195.2365	5.421
52150.9232	-192.0441	5.161
52150.9260	-204.0816	5.099
52150.9288	-209.2001	8.295
52150.9317	-204.1222	6.086
52150.9345	-213.5170	8.890
52150.9373	-217.0743	9.561

7 ROTATIONAL VELOCITIES, MASS RATIO AND INCLINATION ANGLE

Rotational velocities, $V \sin i$, of the secondary star, derived from observations, can lead us to independent estimates of the mass ratio if K_2 is known, and consequently to the semi-amplitude of the primary star (Horne et al. 1986). Furthermore, they can be used to help us estimate the inclination angle of the binary by comparing the variation of $V \sin i$ with orbital phase against models (e.g. Casares et al. 1996). This approach has been made for AE Aqr by the latter au-

Table 8. Orbital Parameters obtained from the absorption lines of AE Aqr for SPM and AAT data, using cross correlations with 61 Cyg A and HR 222 respectively. The sigma values are the rms errors of the sinusoidal fits.

Orbital Parameter	AAT	SPM
γ ($\mathrm{km\,s^{-1}}$)	-69.35 ± 0.97	-63.50 ± 0.35
$K_{\rm abs}$ ($\mathrm{km\,s^{-1}}$)	169.74 ± 1.02	168.72 ± 0.50
$HJD_{\odot}$ (2439030+)	0.951(3)	0.78386(4)
P_{orb} (days)	0.410645(1)	0.41165557(3)
σ	6.96	3.95

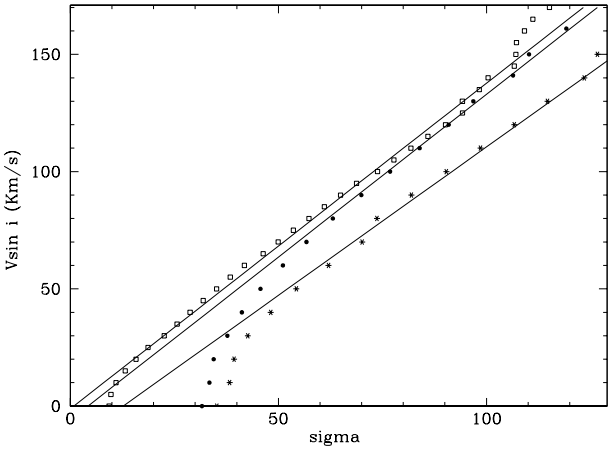

Figure 3. Rotational velocity calibrations derived from the broadening of template stars. The AAT data are shown as open squares. For the SPM data, dots denote the Thomson detector and asterisks the SITe detector. The solid lines correspond to linear fits derived from the data in the 50-100 sigma range only (see text).

thors and also by Welsh et al. (1995), who took a more general approach in the sense that the amplitude of any "ellipsoidal variations" arising from the secondary can be used to constrain the inclination angle, because for a given mass ratio, the amplitude of the variation will depend on the inclination angle of the system. This will be true not only for

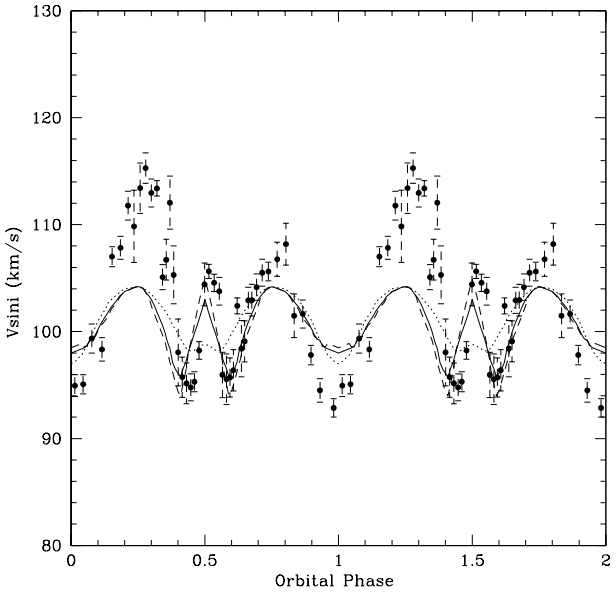

Figure 4. Rotational velocity of the secondary star as a function of orbital phase, obtained from the cross correlations derived from the combined AAT and SPM observations. The error bars are discussed in the text.

rotational velocities, but also for the continuum variations and the observed absorption-line flux as a function of orbital phase. In this section we derive $V \sin i$ from our observations and derive probable values for the mass ratio and inclination angle.

The rotational velocity of the secondary star can be obtained from the width of the cross-correlation function. We attribute the increased width of the correlation function with respect to the intrinsic width of the template star, to the rotational broadening of the secondary star. To convert the calculated sigma of the Gaussian fit to the peak of the CCF to $V \sin\ i$ we have broadened the template stars HR222 and 61 Cyg A with a suitable rotational kernel. The kernel was produced for a range of $V \sin i$ from 10 to $200\,\mathrm{km\,s^{-1}}$ and applied to the IRAF program *convolve* to broaden the template star. The broadened templates are then cross-correlated with the original template and the σ of the Gaussian fit is calculated. We have used a simple broadening function for spherical bodies as described by Gray (1976), using a limb darkening coefficient of $\epsilon = 0.5$ and a bin width corresponding to the spectral resolution of the AAT observations and the two spectral resolutions of the SPM spectra (Thomson and SITe detectors). The resulting calibrations are shown in Figure 3. The symbols are explained in the figure caption.

We have calculated the rotational velocities $V \sin i$ from the measured sigma of the cross correlations, calibrated with the linear fits depicted in Figure 3. We believe this is well justified as the measured sigma values are in the linear region, far from the non-linear points (shown in Figure 3) calculated for lower rotational velocities which, in each case, approach the velocity resolution for each instrumental setup. At some orbital phases, the scatter is large, a result also found by Casares et al. (1996) and by Welsh et al. (1995). As was

also done by these authors, we binned our data to lower the scatter and obtain error estimates. The rotational velocity results are depicted in Figure 4. The error bars are the probable errors, i.e. the standard deviations for the 5 point samples. These values may suffer from small number statistics; also the error estimate assumes that there is no intrinsic variation of $V \sin i$ over 0.02 of an orbit. If there is, we will tend to overestimate the error bar. Although the AAT and SPM data were combined in the binning process, and so cannot be distinguished in Figure 4, we also looked at the unbinned data and it was clear that the two datasets were consistent, so that using them together in the binning was justified. We have produced a mean rotational velocity value for each of 45 bins, of about 0.02 orbital phase width each, by calculating the simple average and standard deviation of a constant sample of 5 data points in each bin. We discarded the 18 SPM spectra taken in September 1997, which were not properly calibrated to convert their sigma into rotational velocities, as well as five other spectra which had a very poor signal-to-noise ratio. In the Figure we observe the basic double modulation expected from an elongated secondary, with low velocities detected at phases 0.0 and around 0.5, and larger values at phases 0.25 and 0.75. The minimum rotational velocity observed in both cases is about $92\,\mathrm{km\,s^{-1}}$ at phase 0.0, when the secondary passes in front of the accretion disc and about the same value near phase 0.4–0.6, when the secondary is behind the primary star. This is expected as these are the phases when we should see a more spherical body. The rotational maxima are asymmetric; the velocities found for phase 0.25 have velocities near $114\,\mathrm{km\,s^{-1}}$, while around phase 0.75 they are about $108\,\mathrm{km\,s^{-1}}$. Another important feature shown in Figure 4 is the behaviour of the rotational velocity between phases 0.4 and 0.6; an inverted V-shaped structure is present, with low velocities at phases 0.4 and 0.6 and a local maximum at phase 0.5. We have also plotted the three computed models of $V \sin i$ by Casares et al. (1996), depicted in their Figure 5, and compared them with our observations. Some major points relating to their models are discussed at the end of this section, and full details can be found in their paper. The overall observed rotational curves show big differences from the results of the models. In general the amplitude is much larger than predicted by the models. Furthermore, the observational data do not behave symmetrically. As mentioned above, the rotational velocities are much larger at phase 0.25 than at phase 0.75, and on the other hand, close to phase 0.0, the observed velocities are much lower than predicted by the models. One feature that is present in both models and observations is the inverted V-shaped structure between phases 0.4 and 0.6. We will also address this point at the end of this section, when we try to estimate the inclination angle.

We can derive the mass ratio of the binary, and consequently the semi-amplitude of the radial velocity curve of the white dwarf, using the rotational velocity of the secondary star. For a Roche-lobe-filling co-rotating secondary star the predicted rotational velocity is:

$$V \sin i/K_2 = (1+q)R_2^{RL}/a, \tag{2}$$

(Horne et al. 1986). Combining this relation with the analytical expression by Echevarría (1983):

$$R_2^{RL}/a = 0.47459[q/(1+q)]^{1/3}, \tag{3}$$

obtained from the tabulations by Kopal (1959), we obtain:

$$V \sin i = 0.475 K_2 q^{1/3}(1+q)^{2/3}. \tag{4}$$

This equation applies to rotating spheres with equivalent radii having the same volume as the contact component. The volume radius is closest to the equatorial radius of the Roche lobe when viewed at conjunction. Then, to a first approximation we can use the observed minimum rotational velocity observed at phase 0.0 of $V(\mathrm{min}) \sin i = 92 \pm 3\,\mathrm{km\,s^{-1}}$, and use the equation above. Taking $K_R = 168.7\,\mathrm{km\,s^{-1}}$ we obtain $q = 0.6 \pm 0.02$. We have taken the same approach as Welsh et al. (1995), but using a slightly different R_2^{RL}/a approximation.

A mass ratio $q = 0.6$ implies $K_1 = 101 \pm 3\,\mathrm{km\,s^{-1}}$, a value which is in excellent agrement with the $K_1 = 102 \pm 2\,\mathrm{km\,s^{-1}}$ determination from the time-delay curve of the 33 s pulsation reported by Eracleous *el al.* (1994).

The inclination angle can be estimated from the amplitude of the rotational velocity curve. Although the curve is highly distorted from the ellipsoidal, or tear-drop, shape of the Roche-Lobe, we can use the maximum and minimum $V \sin i$ at phases 0.75 and 0.0 if we assume they are representative of the ellipsoidal variations (108 and $92\,\mathrm{km\,s^{-1}}$ respectively). Taking these values, we obtain a total amplitude of about 20 percent. We can compare this result with the ellipsoidal variation models by Welsh et al. (1995) which are absorption-line flux models constructed for a limb- and gravity-darkening Roche-Lobe star, using $\beta = 0.08$ for a gravity-darkening given by $T_{\mathrm{eff}} \alpha\, g^{\beta}$. Their models used $q = 0.65$ and a limb-darkening coefficient of $\epsilon = 0.4$, but they found that nearly identical estimates were obtained for $\epsilon = 0.6$. Their model curves are shown in the lower part of their Figure 7 for three inclination angles: 35°, 50° and 65°. The latter solution has an amplitude of about 20 percent in agreement with our observations. Although different observables are being considered, we expect a similar amplitude, because in both cases the maximum (minimum) should occur when the largest (smallest) area is seen, and it is the variation in projected stellar radius that provides the dominant effect. The amplitude is consistent with the ratio of the mean radius to the front-back equivalent Roche-Lobe radius for $q \approx 0.6$ (see Figure 4 in Welsh et al. 1995). Further, an observed amplitude of 20 percent is consistent with the results found by van Paradijs et al. (1989) both from models and from the observed amplitude of the quiescent V-band ellipsoidal variations. Similar results are found in the papers by Chincarini & Walker (1981) and by Bruch (1991). An interesting feature in all these publications is that they show that the ellipsoidal photometric variations are not symmetric; typically, the maximum at phase 0.25 is stronger than the one at phase 0.75 (see for example Figure 4 in van Paradijs, Kraakman H. & van Amerongen 1989), similar to what we find in the rotational velocity curves.

Is there a possible explanation for the asymmetry? There seem to be two possible explanations for a larger amplitude for $V \sin i$ at phase 0.25. One is that there is some additional source of broadening that is stronger on the trailing hemisphere, and the other is that slightly asymmetric irradiation causes the effective radius of the star to be larger on the trailing hemisphere than on the leading one. We shall discuss these possibilities further in Section 12.

Another estimate of the inclination angle can be made

by comparing our observations with the models of Casares et al. (1996). Their models of $V \sin i$ as a function of phase assume a quadratic limb-darkening law and a gravity-darkening law given by $T_{\rm eff}\, \alpha\, g^{\beta}$. They computed 16 sets of models for inclinations and β in the range 40°–70° and 0–0.3 respectively. The other parameters were fixed, with $\epsilon = 0.65$, $T_{\rm eff} = 4500$ K, $K_2 = 162\,{\rm km\,s^{-1}}$ and $q = 0.62$. Their three plotted models (see their Figure 5) are all for $\beta = 0.08$. They find that the synthetic V_{rot} sin i curves exhibit gradual changes in shape and amplitude as the inclination angle increases. Their models are shown in Figure 4 for different inclination angles (dotted line, 40°; solid line 58°; and dashed line 70°). Although the amplitude of the observed variation of V_{rot} sin i as a function of phase is greater than those predicted from their models, it is evident that the V-shaped structure increases in strength with the inclination angle. Taking this into account, we believe that an inclination close to 70° yields a better fit to our data than the other values. The more elaborate Roche Tomography of Watson et al. (2006), which effectively takes two of the pieces of information we have been using, the variation in line velocity and line shape/width, and adds a third, the variation in line flux, which we do not have at our disposal in this paper, allows them to construct surface maps of the secondary star, from which they determine the most accurate system parameters. In particular they calculate an inclination angle of 66°, close to our result. Indeed, these authors refer to an unpublished version of this paper, to support their result on the inclination angle. It is satisfactory that the different methods used to obtain the inclination of this binary are now in generally good agreement. We note that the preferred value is now very close to the upper limit of 70° imposed by the lack of eclipses (Robinson et al. 1991).

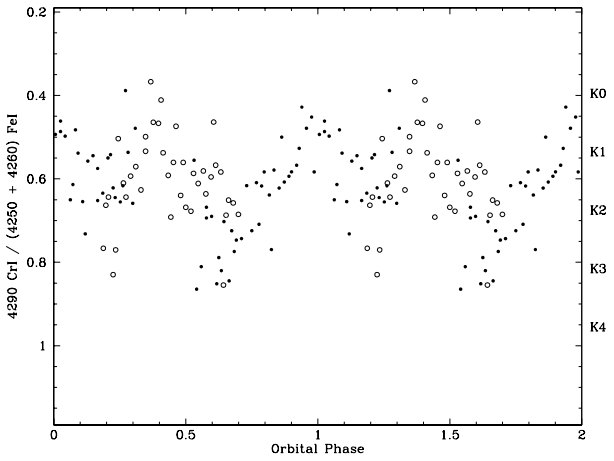

Figure 5. The absorption line ratio Fe I/Cr I as a function of orbital phase for the AAT observations. This line ratio is a basic temperature indicator for K stars (see text). A first order calibration of the spectral type, using the spectral template stars, is shown at the right.

8 SPECTRAL TYPE AS A FUNCTION OF ORBITAL PHASE

The AAT spectra have the highest spectral resolution and best signal-to-noise ratio for measuring the line depths of the Fe I $\lambda\lambda$4250, 4260 and Cr I λ4290 absorption lines. These lines are amongst those recommended for spectral classification in K stars by Keenan & McNeil (1976) because the atoms belong to the same abundance group and so the line ratios define spectral type (or effective temperature) essentially independently of metallicity. We have done this both for the individual AE Aqr spectra and for the comparison stars. Figure 5 shows the line ratio Fe I$\lambda\lambda$4250, 4260/Cr Iλ4290 as a function of orbital phase. A first order calibration of this line ratio with the same line ratio measured in the spectral standards (see Table 1) was made. This is shown on the right hand side of the diagram. We observe that the line ratio has a roughly double sinusoidal behaviour with two minima and two maxima. It is important to note that the system appears to have an earlier spectral type (about K0), close to phases 0.4 and 0.9 and a tendency to move to later spectral types towards phase 0.2 (about K2) and phase 0.65 (close to K4). These changes in absorption line strengths may be due to irradiation effects (see Warner 1995 and references therein), or star-spots on the secondary star (Watson et al. 2006). These effects as well as the changes in temperature as a function of phase will be discussed in section 12.

9 THE FUNDAMENTAL PARAMETERS OF AE AQR

Assuming that the radial velocity semi-amplitudes reflect accurately the motion of the binary components, then from our results: $K_{em} = K_1 = 101 \pm 3\,{\rm km\,s^{-1}}$; $K_{abs} = K_2 = 168.7 \pm 1\,{\rm km\,s^{-1}}$, and adopting $P = 0.4116554800$ d we obtain:

$$M_1 \sin^3 i = \frac{PK_2(K_1+K_2)^2}{2\pi G} = 0.52 \pm 0.03 M_{\odot}, \qquad (5)$$

$$M_2 \sin^3 i = \frac{PK_1(K_1+K_2)^2}{2\pi G} = 0.31 \pm 0.02 M_{\odot}, \qquad (6)$$

and

$$a \sin i = \frac{P(K_1+K_2)}{2\pi} = 2.19 \pm 0.02 R_{\odot}. \qquad (7)$$

Assuming an inclination angle $i = 70° \pm 3°$, the system parameters become: $M_1 = 0.63 \pm 0.05\, M_{\odot}$; $M_2 = 0.37 \pm 0.04\, M_{\odot}$; and $a = 2.33 \pm 0.02\, R_{\odot}$.

10 THE $M_1 - M_2$ DIAGRAM

A convenient tool for the analysis of the masses and inclination angle of the binary has been developed by Echevarría et al. (2007). This M_1 – M_2 diagnostic diagram is shown in Figure 6. In this diagram, the slope of the straight lines is simply given by q and therefore, for a given value of M_1, we have a corresponding value of M_2. The vertical dashed area indicates a neutron star regime, set at the left by the white dwarf Chandrasekhar limit. The horizontal upper region shows the values obtained from the empirical M_2–P_{orb} relations by Warner (1995, page 111) and Echevarría (1983). These two relations, using the improved orbital period, give $M_2 = 1.14\,M_\odot$ and $M_2 = 1.07\,M_\odot$ respectively. The spectral types labelled on the left side of the diagram correspond to the ZAMS stellar models discussed by Kolb & Baraffe (2000), while those shown on the right side correspond to evolved stars that are still within the main sequence band (see Kolb & Baraffe 2000 for detailed explanations). Points in the white area are then within these limits as we expect that the primary star will not exceed the Chandrasekhar limit, and that the secondary star will not be on the MS (Echevarría 1983; Beuermann et al. 1998). From the three selected mass ratios ($q = 0.7$, 0.65 and 0.6), and possible inclination angles ($i = 58°, 66°$ and $70°$), values which are consistent with most of the published observations shown in Table 9, we conclude that the white dwarf is probably not a very massive primary, with an upper limit of about $M_1 = 1.0\,M_\odot$ (for $i = 58°$) and a lower limit of $M_1 = 0.63\,M_\odot$ (for $i = 70°$). The observational evidence for a high inclination angle from Robinson et al. (1991), from Watson et al. (2006) and from this paper suggests that we may be closer to the lower mass limit. This is also consistent with the expected lower limit of $0.6\,M_\odot$ for a Helium White Dwarf, in order to support the 33 s pulsations (Robinson et al. 1991). Moreover, the observed spectral type is inconsistent with the predicted values in the diagram, except for the case of a high mass ratio and low inclination angle solution compared with evolved main-sequence stars. Furthermore, the possible values for the mass of the secondary are very different from those of a main sequence star, as they are far from the upper gray zone in the diagram. This indicates that we are dealing with a late-type star which is under-massive for its size or (more plausibly) over-sized for its mass. Although this conclusion is not new, and has been pointed out as early as Crawford & Kraft (1956); Patterson (1979) and Echevarría (1983), and later by other authors (see references in Table 9 and further discussion in the next section), it is presented here in the formal context of the M_1 – M_2 diagnostic diagram.

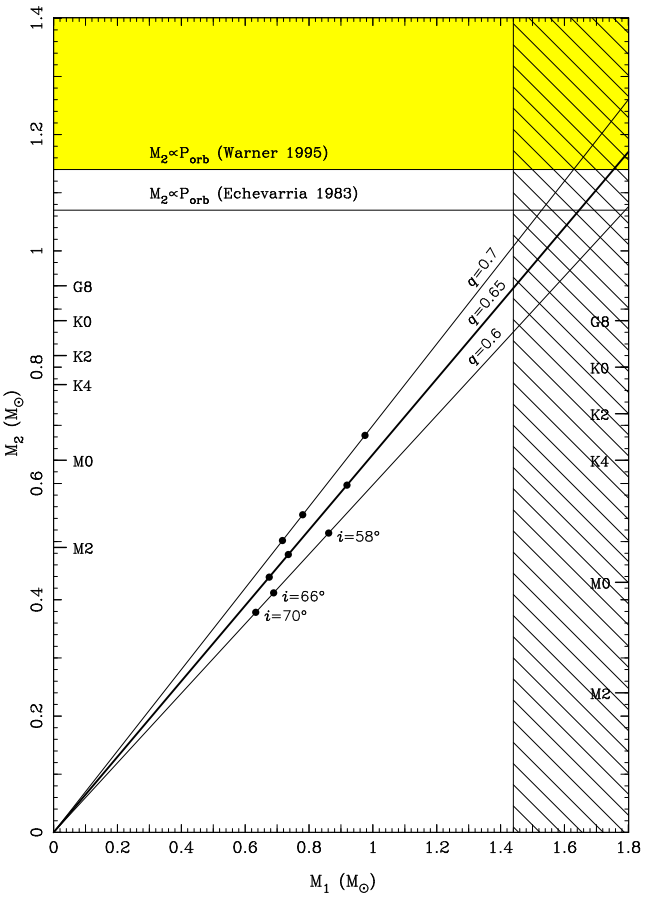

Figure 6. $M_1 - M_2$ mass diagram for AE Aqr. The components must lie in the lower left quadrant of the diagram. The spectral type of the secondary would be given by the labels on the left-hand axis if it were a ZAMS star, or by the labels on the right-hand axis if an evolved MS star; see text for details.

11 THE RADIUS OF THE SECONDARY

Following our results we can compare the mass and radius of the secondary with those of normal main sequence stars. Using the mass-radius relation for main sequence stars:

$$R/R_\odot = 1.057(M/M_\odot)^{0.906} \quad (8)$$

by Echevarría (1983), and taking the derived mass of the secondary $M_2 = 0.37\,M_\odot$ in this paper, we obtain a radius $R_2^{ms} = 0.43\,R_\odot$. On the other hand, using eq.(3) we obtain:

$R_2^{RL}/a = 0.34$, and taking our result on the separation of the binary $a = 2.33\,R_\odot$, we obtain $R_2^{RL} = 0.79\,R_\odot$. Taking the ratio $f = R_2^{RL}/R_2^{ms}$ we obtain a value of 1.84. We will call this ratio the filling factor. Therefore the secondary star appears to have a radius larger than a star of that mass on the main sequence by nearly a factor of two. We have followed the same procedure for all entries in Table 9 (see next section), calculating first R_2^{ms} from eq.(8) and the binary separation a from eq. (7), while R_2^{RL} has been derived from eq.(3), taking, in both calculations, the corresponding values in Table 9. The results are also shown in Table 9.

12 DISCUSSION

Table 9 shows the fundamental parameters of the binary, obtained by several authors since the early work by Joy (1954). Columns (1) to (14) show: the period; the measured (and assumed) semi-amplitudes K_2 and K_1 for the secondary and primary stars respectively; the mass ratio q and the estimated inclination angle i; the binary separation a (which has been calculated here when necessary); the projected rotational velocity of the secondary; the masses of the secondary and primary components; the Roche-Lobe radius R_2^{RL} and the corresponding main-sequence radius, based on the estimated mass of the secondary; the filling factor f; the estimated spectral type and the references to the authors. We can observe in the Table a certain trend with time. Since the first observations by Joy (1954), there is a slight tendency towards larger radial velocity semi-amplitudes for the secondary star, a stronger tendency for lower values for the primary star, and hence a steady decrease in mass ratio. The secondary radii and calculated filling factors depend strongly on the mass of the primary and on the mass ratio, and therefore there is also a decrease in the main-sequence radius and an increase in the filling factor. These tendencies cannot be attributed to real changes with time, but rather to a refinement in the measured parameters as a result of better observing techniques and the use of instruments with higher spectral resolutions. The latest results, by Watson et al. (2006) and this paper, differ mainly because of the adoption of different values for the semi-amplitude of the primary star. These estimates are derived from two new techniques: the entropy landscape and the rotational velocity of the secondary respectively. Although entropy maps do in principle give the most "accurate" values of orbital parameters, their errors are very difficult to assess properly, because enormously time-consuming Monte-Carlo calculations would be needed (Watson et al. 2006; see, however, Watson et al. 2007 for a way of estimating the error). On the other hand, our result for K_{wd} depends on an educated guess as to which is the rotational velocity that gives the least-deformed secondary, among the values of this complex and variable parameter as a function of orbital phase. However, our result is in good agreement with the results by Eracleous et al. (1994), based on the independent $K_{\rm pulse}$ estimate. We have obtained also a very large filling factor, greater than previously estimated. Such an increase in the radius of the secondary star could be explained through X-ray heating mechanisms discussed by Hameury et al. (1993), while evolved main sequence star scenarios will also yield a significantly larger stellar radius (Kolb & Baraffe 2000); in addition, any mass-transferring star is likely to be out of thermal equilibrium, increasing the radius as a result.

The paper by Watson et al. (2006) only quotes explicitly the values for the masses and inclination that the authors deduce from their entropy landscape technique. This technique uses the currently most sophisticated procedure to allow for the variation in intensity over the surface of the secondary, and their results are probably the most reliable ones in Table 9. To enable us to compare their results with our own, and with previously published results, we have used their masses and inclination, together with equations (3) to (8) in the present paper, to compute the other entries in their row of Table 9; these entries are in italics to emphasise that they have been derived by us and are not quoted in their paper (the spectral type of K4 is assumed in their paper, so is not in italics). The most noticeable difference is that the K_1 value deduced from their paper is significantly larger than ours and than the K_1 deduced from spin pulse measurements (Eracleous et al. 1994).

As discussed in Section 5, the observed radial velocity residuals seem to be explicable by a combination of irradiation effects on the hemisphere of the secondary facing the white dwarf and some form of enhanced absorption on the averted hemisphere.

A full discussion on whether the radial velocity semi-amplitude of the secondary star in a cataclysmic variable increases with irradiation or back-illumination effects, or decreases with line quenching, has been made by several authors (e.g. Wade 1981; Martin 1988; Friend et al. 1990). However, in the case of AE Aqr an estimation of this effect is not easy to obtain. We found that, from the published results shown in Table 9, only Watson et al. (2006) make a correction, based on the entropy landscape technique. Although they do not give an explicit value for the corrected K_2, it is possible, as discussed above and shown in Table 9, to derive it from their given masses and inclination angle. Since they quote an uncorrected $K_2 = 168.4 \pm 0.2\,{\rm km\,s^{-1}}$ value, we estimate that their correction amounts to $0.8\ {\rm km\,s^{-1}}$ only. We are unable to make a proper correction to our data, due to the complex behaviour of the velocity residuals shown in Figure 2 and discussed in Section 5. Whether or not the underlying sinusoid in Figure 1 may be a reasonable representation of the orbital motion or not, nevertheless, our uncorrected K_2 result does not differ greatly from the corrected value by Watson et al. (2006). Here, we may safely assume that our K_1 result, based on the mass ratio deduced from the rotational velocities and the semi-amplitude of the secondary, will not be significantly affected. We can indeed use their "corrected" K_2 value in equation (4) and obtain essentially the same result for K_1 as we find from our uncorrected value of K_2.

Irradiation effects near the inner Lagrangian point were also found by Watson et al. (2006), and they could partially explain the complex temperature behaviour as a function of orbital phase. At phase 0.0 we would observe an unirradiated hemisphere of the secondary with a temperature equivalent to a K0 star. However, where irradiation effects are important, there may be a quenching effect on the Fe I absorption lines greater than on the Cr I lines, producing (paradoxically) an apparent decrease in temperature and moving the spectral type to later classes on the irradiated hemisphere. The source of the enhanced absorption is harder to under-

Table 9. Comparison of Fundamental Parameters of AE Aqr

P_{orb} (days)	K_2	K_1 ($\mathrm{km\,s^{-1}}$)	q	i (°)	a ($R_\odot$)	$V_{rot}\sin i$ ($\mathrm{km\,s^{-1}}$)	M_2 ($M_\odot$)	M_1 ($M_\odot$)	R_2^{RL} ($R_\odot$)	R_2^{ms} ($R_\odot$)	f	Sp. Type	Authors
0.7007	146	151	1.03									dK0	J54
0.4118[a]	162.5	145	0.89										PG69
0.4116550	162.5[b]	129*	0.79	58	2.80		0.74	0.94	1.01	0.80	1.27	K5V	P79
0.4116537	159	135	0.85	64	2.66		0.69	0.82	0.98	0.75	1.31	K5V	CW81
0.4116580	160[c]	141	0.88	63^-	2.75		0.76	0.88	1.01	0.82	1.23	K5V[h]	RSB91
0.4116580	160[c]	141	0.88	70^+	2.60		0.65	0.75	0.96	0.71	1.35	K5V[h]	RSB91
0.41165561	159	122[d]	0.78	57	2.72		0.70	0.91	0.98	0.76	1.29	K3V	RB94
0.411655601[c]	157.9[e]	102[f]	0.65	55	2.58	85-108	0.57	0.89	0.90	0.63	1.43	K3-K5	WHG95
0.411655653	162.0	102[f]	0.63	58	2.53	101	0.50	0.79	0.88	0.56	1.57	K4	CMMH96
0.411655653	*167.6***	*113.3***	0.68	66	*2.50***	*99***	0.50	0.74	*0.88***	*0.56***	*1.57***	K4	WDS06
0.4116554800	168.7	101[g]	0.60	70	2.33	92	0.37	0.63	0.79	0.43	1.84	K0-K4	This paper

Adopted from a) Walker (1965); b) Payne-Gaposchkin (1969); c) from Feldt & Chincarini (1980); d) from K_{pulse} by Robinson et al. (1991); e) from Welsh et al. (1993); f) from K_{pulse} by Eracleous et al. (1994); g) derived from our measured rotational velocity and deduced mass ratio (see Section 7); h) Chincarini & Walker (1981); *) pulse arrival method. **) Inferred from their entropy landscape results – see text for details. -) minimum and +) maximum inclination angle limits.
References: J54: Joy (1954); PG69: Payne-Gaposchkin (1969); P79: Patterson (1979); CW81: Chincarini & Walker (1981); RSB91: Robinson et al. (1991); RB94: Reinsch & Beuermann (1994); WHG95: Welsh et al. (1995); CMMH96: Casares et al. (1996); WDS06: Watson et al. (2006). The results by Watson et al. (2006) are the only ones that make a correction for the effects of variable intensity over the surface of the secondary.

stand. Although Watson et al. (2006) found strong evidence for a spotted region at high latitude on the secondary, at a longitude that corresponds to its being on the meridian roughly at orbital phase 0.25, there is no sign in their Roche tomograms of any enhanced absorption on the averted hemisphere. The source of the enhanced absorption that seems to be required by the velocity residuals thus remains uncertain, but is probably not a starspot, at least in the sense used by Watson et al. (2006).

Can we relate the variations of $V\sin i$ with orbital phase, shown in Figure 4, to the variations in the radial velocity, and gain any further information about the region of enhanced absorption? Certainly, the amplitude of the variations, especially around phase 0.25, is larger than expected from straightforward models of the effect of varying projected radius. In other words, around orbital phases 0.25 and 0.75 the absorption lines appear to be broader than expected. Irradiation can perhaps account for the *asymmetry* between these phases, for example if the leading hemisphere were hotter than the trailing one (as found for several CVs by Davey & Smith 1992; see also Smith 1995) then the absorption lines would be quenched preferentially on the leading hemisphere, near the L_1 point, and the line would appear somewhat narrower (smaller effective $V\sin i$) at phase 0.75 than on the trailing hemisphere at phase 0.25. However, it is hard to see how irradiation could ever cause the absorption lines to appear broader than expected from a purely geometrical effect. The larger-than-expected amplitude of the curve in Figure 4 seems to require some additional source of broadening, or some intensification of the line that has the same effect when it comes to measuring $V\sin i$. A region of enhanced absorption on the averted hemisphere, centred some 180° in longitude away from the L_1 point, might provide this, as well as accounting for the velocity residuals in Figure 2. However, this sheds no additional light on the source of the enhanced absorption. The other possible explanation for the large amplitude is that there is some additional physical mechanism operating that adds to the width of the line, such as turbulence, but it would need to be anisotropic, so that the broadening effect was enhanced at the quadratures; there is no obvious reason why that should be so.

We conclude that our observations are consistent with, and indeed seem to require, a region of enhanced absorption on the averted hemisphere of the secondary star, but that they provide no convincing evidence for the source of that absorption.

13 CONCLUSIONS

High-dispersion time-resolved spectroscopy of the cataclysmic variable AE Aqr was obtained during several observing runs over a ten-year period. The high spectral resolution coupled with the high signal-to-noise ratio obtained for the strong absorption lines allows us to find several fundamental parameters of the binary. The radial velocity analysis yields a semi-amplitude value of $K_{abs} = 168.7 \pm 0.5\,\mathrm{km\,s^{-1}}$ for the secondary star and a systemic velocity of $-63\,\mathrm{km\,s^{-1}}$. A new ephemeris was calculated by expanding the 39-y radial velocity database of Welsh et al. (1995) to 58 y with new observations by Reinsch & Beuermann (1994), Casares et al. (1996) and this paper. We have measured the absorption strengths and line ratio of Fe I$\lambda\lambda$4250, 4260/Cr Iλ4290 and made a first order calibration with spectral type, using the spectral template stars. The line ratio varies as a function of orbital phase, equivalent to a variation from K0 to K4 with a mean value of K2. The rotational velocity of the red star has been measured as a function of orbital period and shows ellipsoidal variations at twice the orbital frequency. Using the models by Casares et al. (1996) we estimate an inclination angle close to $i = 70°$. The rotational velocities are used to constrain the system mass ratio and yield a white dwarf semi-amplitude value of $K_{em} = 101\,\mathrm{km\,s^{-1}}$ consistent with the derived value from the spin-pulse results by Eracleous et al. (1994). From these values we estimate the masses of the binary as $M_1 = 0.63 \pm 0.05\,M_\odot$; $M_2 = 0.37 \pm 0.04\,M_\odot$; and

a separation of $a = 2.34 \pm 0.02\,R_\odot$. An analysis using the $M_1 - M_2$ diagram points towards a secondary star which is over-sized for its mass, with a radius greater than that of a normal main sequence star by a factor of almost two. Finally, we discuss the measured temperature and spectral variations as a function of orbital phase and suggest that these may be the result of changes in the observed line ratios due to the presence of regions of enhanced irradiation, near the inner Lagrangian point but perhaps preferentially on the leading hemisphere of the secondary, and of enhanced absorption on the averted hemisphere. The asymmetry in the variation of the rotational velocity with orbital phase may also be related to the presence of these regions. We currently have no physical model for the region of enhanced absorption, but it needs to produce absorption lines that are abnormally deep or broad, or both.

ACKNOWLEDGMENTS

We are grateful for the use of the facilities at the Anglo-Australian Telescope on Siding Spring mountain, operated by the Anglo-Australian Observatory, and at the 2.1-m telescope at San Pedro Mártir, operated by the Mexican Observatorio Astronómico Nacional. We acknowledge the use of software developed by the UK Starlink project and by the NOAO. We thank the referee for very careful and detailed comments that have led to significant improvements in the paper.

REFERENCES

Bastian T.S., Dulk G.A., Chanmugam G., 1988, ApJ, 324, 431
Beuermann K., Baraffe I., Kolb U., Weichhold M., 1998, A&A, 339, 518
Bookbinder J.A., Lamb D.Q., 1987, ApJ, 322, L131
Bowden C.C.G. et al., 1992, Astroparticle Physics, 1, 47
Bruch A., 1991, A&A, 251, 59
Casares J. Mouchet M., Martinez-Pais I.G., Harlaftis E.T., 1996, MNRAS, 282, 182
Chincarini G., Walker M.F., 1981, A&A, 104, 24
Crawford, J.A., Kraft, R.P., 1956, ApJ, 123, 44
Davey S.C., Smith R.C., 1992, MNRAS, 257, 476
Echevarría J., 1983, RMAA, 8, 109
Echevarría J., Michel R., Costero R., Zharikov S., 2007, A&A, 462, 1069
Eracleous M., Horne K., Robinson E.L., Zhang E-H., Marsh T.R., Wood J.H., 1994, ApJ, 433, 313
Evans D.S., 1967, in Batten, A.H., Heard, J.F., eds, Proc. IAU Symp. 30, Determination of radial velocities and their applications. Academic Press, London, p. 57
Evans D.S., Menzies A., Stoy R.H., 1957, MNRAS, 117, 534
Feldt A.N., Chincarini G., 1980. PASP, 92, 528
Flynn C., Freeman K.C., 1993. A&AS, 97, 835
Friedjung M., 1997, New Astron. 2, 319
Friend M.T., Martin J.S., Smith R.C., Jones, D.H.P., 1990, MNRAS, 246, 637
Gray D.F., 1976, The Observations and Analysis of Stellar Photospheres. Wiley-Interscience, New York, p.398
Hameury J.M., King A.R., Lasota J.P., Raison F. 1993, A&A, 277, 81
Hoffleit D. 1964, Catalogue of bright stars, Third revised edition. Yale University Observatory, New Haven, Conn.
Horne K., Wade R., Szkody P., 1986, MNRAS, 219, 791
Houk N. 1982, Catalogue of two-dimensional spectral types for the HD stars, Vol. 3. Michigan spectral survey, Ann Arbor, Dep. Astron. Astrophys., Univ. Michigan
Houk N., Smith-Moore, M., 1988, Catalogue of two-dimensional spectral types for the HD stars, Vol. 4. Michigan spectral survey, Ann Arbor, Dep. Astron. Astrophys., Univ. Michigan
Johnson H.L., Morgan W.W., 1953, ApJ, 117, 313
Joy A.H. 1954, ApJ, 120, 377
Keenan P.C., McNeil R.C. 1976, An Atlas of Spectra of Cooler Stars: Types G, K, M, S and C. The Ohio State University Press, Columbus, Ohio
Kolb U., Baraffe I., 2000, NAR, 44, 99
Kopal Z. 1959, Close Binary Systems. Chapman and Hall, London
Martin, J.S., 1988, *DPhil thesis*, University of Sussex
Meintjes P.J. et al. 1992, ApJ, 401, 325
Morgan W.W., Keenan P.C., 1973, ARA&A, 11, 29
Morgan W.W., Keenan P.C., Kellman, E., 1943, An atlas of stellar spectra with an outline of spectral classification. Astrophys. Monographs, Univ. Chicago Press.
Patterson J., 1979, ApJ, 234, 978
Payne-Gaposchkin C., 1969, ApJ, 158, 429
Reinsch K., Beuermann K., 1994, A&A, 282, 493
Robinson E.L, Shafter A.W., Balachandran, S., 1991, ApJ, 374, 298
Roman N.G., 1952, ApJ, 116, 122
Roman N.G., 1955, A&AS, 2, 195
Smith R. C., 1995, in Buckley D.A.H., Warner, B., eds, ASP Conf. Series 85, Cape Workshop on Magnetic Cataclysmic Variables. Ast. Soc. Pacific, San Francisco, p. 417
van Paradijs J., Kraakman H., van Amerongen S., 1989, A&AS, 79, 205
Wade, R. A., 1981, ApJ, 246, 215
Walker M.F., 1965, Sky and Telescope, 29, 23
Warner B., 1995, Cataclysmic Variable Stars. Cambridge University Press, Cambridge
Watson C.A., Dhillon V.S., Shahbaz T., 2006, MNRAS, 368, 637
Watson C.A., Steeghs D., Shahbaz T., Dhillon V.S., 2007, MNRAS, 382, 1105
Welsh W.F., Horne K., Gomer R., 1993, ApJ, 410, L39
Welsh W.F., Horne K., Gomer R., 1995, MNRAS, 275, 649
Wilson R.E., 1953, Gen. Cat. of Stellar Rad. Vel. Carnegie Inst. Washington, D.C., Publ No. 601
Wilson O.C., 1962, ApJ, 136, 793
Wynn G.A., King A.R., Horne K., 1997, MNRAS, 286, 436
Zinner E., 1938, Astron. Nach., 265, 345

This paper has been typeset from a TEX/ LATEX file prepared by the author.